Simulation of a Bio-Inspired Swimming Mechanism

T.G. Vlogman*, S. Mohanty, S. Misra

University of Twente, Faculty of Engineering Technology, Drienerlolaan 5, 7522 NB, Enschede, The Netherlands
**corresponding author t.g.vlogman@student.utwente.nl*

ABSTRACT: Remotely actuated synthetic micro-swimmers have many medical applications such as targeted drug delivery and non-invasive surgery. This paper investigates the influence of structural resonances on the propulsion of bio-inspired micro-swimmer designs in a traveling wave acoustic field. A second-order perturbation approach was used to model and solve for the first order time-harmonic and second order acoustic streaming fields and to evaluate propulsive forces on the swimmer. Actuation of the swimmer at its resonance frequencies is found to influence these propulsive forces in a direction dependent on the excited swimmer mode shape. This suggests a possibility for controlling the direction of movement of micro-swimmers remotely based on actuation frequency.

Key words: acoustics, targeted drug delivery, micro swimmer, streaming, acoustic radiation force, propulsion

1 INTRODUCTION

A great diversity of propulsion mechanisms can be observed in nature on a variety of scales. Of special interest in medical applications are swimming mechanisms that operate at the micro scale. Micro-robots that can be maneuvered precisely in biological environments would have tremendous applications in medical care, for example in targeted drug applications. The physics of swimming at micro-scale are very different from those occurring at larger scales [1]. At such small scales the Reynolds number is very low, meaning that viscous forces dominate over inertial forces [2]. This presents a challenge in finding suitable methods of propulsion of micro-robots as the propulsion methods commonly employed at larger scales cannot be used. Whereas in the high Reynolds number flows of ships or fish in water the swimming motion can be reasonably decomposed into a propulsive force due to inertial effects and a counter-acting drag force due to viscous contributions, both the propulsive and resistive forces in low Reynolds number flows originate from viscous effects. Illustrative of the dissimilarity of propulsion at high and low Reynolds numbers is that any sort of reciprocal motion such as that employed by, for example, scallops cannot produce any nonzero time-averaged displacement in a low Reynolds number flow as illustrated in the paper by Purcell [3].

Acoustics have been successfully used to manipulate particles in a fluid by a variety of mechanisms [4]. The two main acoustofluidic forces on particles in a fluid are the acoustic radiation force and the Stokes' drag force, of which the relative magnitude is determined by particle size as described by Lamprecht [5]. Many current acoustic particle manipulation methods rely on generating standing wave fields within a channel containing the particles. A downside of this is the strong dependence on channel geometry to accurately control particle movement. For in-,vivo applications such control of channel geometry is in general not possible.

Recent research by Ahmed [6] found that structural resonances can be used to induce propulsive forces on a micro-swimmer in a traveling wave field. This is a promising area of study as such a traveling wave field is largely independent of channel geometry. However the exact mechanism responsible for the propulsive forces in this situation remains unclear. This paper aims to investigate the relationship between structural resonances and propulsive forces on a swimmer in a traveling acoustic wave field by means of FEM simulations in COMSOL multiphysics software. Special attention is paid to the influence of geometry and swimmer dimensions.

2 METHODOLOGY

The numerical simulations performed consist of a structural analysis, the addition of acoustics and

finally a simulation of the entire acoustofluidic problem. To reduce computational load all analyses were performed in 2D. All simulations were carried out using COMSOL multiphysics 5.3a software with the solid mechanics, pressure acoustics, thermoviscous acoustics and laminar flow interfaces.

2.1 Structural analysis

The structural analysis serves to investigate swimmer vibrational modes when excited by a harmonic perturbation of varying frequency. Various swimmer geometries were created using the CAD software SolidW.orks and then imported into COMSOL multiphysics simulation software. Two main variations in geometry were explored: variation in swimmer tail size and the addition of sharp-edged protrusions to the head of the swimmer. Three swimmer lengths from 180μm to 380μm were simulated as well as two designs of 180μm in length utilizing small and large protrusion sizes. These will be referred to as the stingray I and stingray II designs respectively. An overview of the designs can be seen in figure 1. In the simulations the swimmer's material properties were taken to be that of PDMS as listed in table 2 in appendix A. A small amount of internal damping was added which was modeled as proportional damping. Damping coefficients of 0.01 were chosen on the first two asymmetric mode eigenfrequencies.

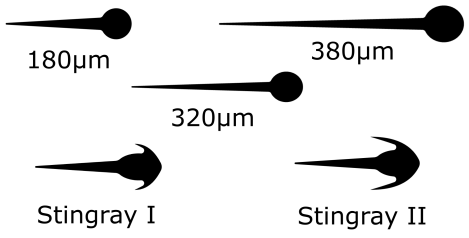

Fig. 1: Geometry of the simulated swimmers

The eigenfrequencies and the corresponding eigenmodes of each swimmer design were determined using COMSOL's eigenfrequency study. Of these modes the ones showing an asymmetric swimmer motion are most relevant as these should theoretically provide a propulsive force if the swimmer were immersed in a viscous medium.

In order to assess the magnitude of the deformation when the swimmers are excited in or around their eigenfrequencies a frequency sweep was carried out. In this study a harmonic load was placed on one side of the swimmer to simulate the situation of excitation by sinusoidal acoustic waves. Elastic strain energy was used as a measure of deformation magnitude.

2.2 Acoustics

Following the structural analysis the model was extended to examine the effects of acoustic actuation. This was done by modeling a 1500μm by 1000μm rectangular domain filled with water representing the medium around each swimmer using the pressure acoustics module in COMSOL. Plane-wave radiation boundary conditions were imposed upon the top and bottom sides of the domain to simulate incoming and exiting acoustic waves. To mimic the situation of acoustic waves propagating in the lateral direction of the swimmer the sides of the medium were assigned hard boundary wall conditions.

On the bottom side of the medium the incoming acoustic waves were modelled using an incident pressure field boundary condition. Pressure variations of the form $p(x,t) = p_0 sin(\omega_0 t)$ were applied in which p_0 and ω_0 represent the pressure amplitude and angular excitation frequency respectively. In this case a value of 10MPa was used for p_0 and ω_0 was varied between 1kHz and 100kHz.

To determine whether the asymmetric motion of the eigenmodes found in the structural analysis can be successfully induced using acoustics a frequency domain study was carried out. First the eigenfrequencies of the swimmer were once again determined using an eigenfrequency study, this time with the surrounding medium. Then the frequency response was determined by sweeping ω_0 over a range of values encompassing these eigenfrequencies.

2.3 Fluids

Finally the complete acoustofluidic problem was simulated to investigate streaming patterns and evaluate propulsive forces on the swimmer. In the following a brief explanation of the physics and mathematics involved will be given followed by the implementation in COMSOL.

2.3.a Governing equations

The governing equations for the fluid medium are the continuity equation and the Navier-Stokes equation:

$$\frac{\partial \rho}{\partial t} + \nabla \cdot (\rho \vec{u}) = 0 \tag{1}$$

$$\frac{\partial}{\partial t}(\rho\vec{u}) + \rho(\vec{u}\cdot\nabla)\vec{u} = -\nabla p + \mu\left[\nabla^2\vec{u} + (\frac{1}{3}+\mu_b)\nabla(\nabla\cdot\vec{u})\right] \tag{2}$$

where ρ is the mass density, $\vec{u}$ is the velocity and p is the fluid pressure. μ represents the dynamic viscosity and μ_b ratio of dynamic to bulk viscosity $\mu_b = \mu_B/\mu$. Solving these nonlinear partial differential equations numerically on a sufficiently fine mesh would require tremendous computing power. A common approach to simplify the calculations is to apply a second-order perturbation approach as described in the paper by Bruus [7] in which the velocity, pressure and density fields are assumed to have the form of:

$$\vec{u} = \vec{u_1} + \vec{u_2} \tag{3}$$

$$p = p_0 + p_1 + p_2 \tag{4}$$

$$\rho = \rho_0 + \rho_1 + \rho_2 \tag{5}$$

where the subscript 0, 1 and 2 denote the quiescent, first order and second order terms respectively. In the equations (3), (4) and (5) the first order terms correspond to the time-harmonic acoustic perturbations and the second order terms are due to acoustic streaming effects. These streaming effects arise due to the nonlinear terms in the Navier-Stokes equations [7]. Physically their origin is explained by the viscous attenuation of sound waves as they travel through a medium and interact with boundaries [8].

By linearizing equations (1) and (2) it is possible to solve for the first and second order fields separately and use superposition to determine the complete approximate solution. Due to the time-harmonic nature of the first-order quantities the first-order fields can be assumed to be of the form $e^{i\omega t}$ as described in the book by Mason [9]. The nonlinear terms omitted in the first order equations are then used as source terms in the second order equations.

The linearized continuity and Navier-Stokes equations applied to the first-order fields are given by the equations:

$$\frac{\partial \rho_1}{\partial t} + \rho_0 \nabla \cdot \vec{u_1} = 0 \tag{6}$$

$$\rho_0 \frac{\partial \vec{u_1}}{\partial t} = -\nabla p_1 + \mu\left[\nabla^2\vec{u_1} + (\frac{1}{3}+\mu_b)\nabla(\nabla\cdot\vec{u_1})\right] \tag{7}$$

where the two nonlinear terms $-\nabla \cdot (p_1\vec{u_1})$ and $\rho_1(\partial\vec{u_1}/\partial t) + \rho_0(\vec{u_1}\cdot\nabla)\vec{u_1}$ which have been omitted in equations (6) and (7) will be used as source terms for the second order equations.

As the second-order acoustic streaming fields are steady, evaluating these on the microsecond timescale of the acoustic oscillations is not of interest. This simplifies the problem to first solving the first-order equations in the frequency domain and then solving the time-averaged second order equations. The time-averaged second order continuity and Navier-Stokes equations are given by:

$$\rho_0 \nabla \cdot \langle \vec{u_2} \rangle = -\nabla \cdot \langle \rho_1 \vec{u_1} \rangle \tag{8}$$

$$-\nabla p_2 + \mu\left[\nabla^2\vec{u_2} + (\frac{1}{3}+\mu_b)\nabla(\nabla\cdot\vec{u_2})\right] = \left\langle \rho_1 \frac{\partial \vec{u_1}}{\partial t} \right\rangle + \rho_0 \langle (\vec{u_1}\cdot\nabla)\vec{u_1} \rangle \tag{9}$$

where the angle brackets indicate a time-averaged value over one oscillation period. The time-averaged harmonic first order quantities can be calculated using the real-part rule:

$$\langle f(t)g(t) \rangle = 0.5Re\left[\overline{f(t)}g(t)\right] \tag{10}$$

in which the overbar indicates the complex conjugate. These second order equations can then be used to model the steady-state acoustic streaming fields that result from the nonlinear effects in the first-order acoustic problem.

After solving for the first and second order fields the forces by the fluid on the swimmer can be evaluated.

In general the force on an object immersed in a fluid medium can be calculated using:

$$F = \int_{S(t)} (\boldsymbol{\sigma} \cdot \vec{n}) dS \tag{11}$$

where the bold face indicates a tensor quantity. In equation (11) $\boldsymbol{\sigma}$ is the stress tensor and $\vec{n}$ is the unit normal vector pointing from the surface of the object $S(t)$ towards the fluid. Applying this to the situation of the swimmer and making use of the perturbation theory approach this force can be time-averaged and divided into first and second order contributions:

$$\langle F \rangle = \left\langle \int_{S(t)} (\boldsymbol{\sigma_1} \cdot \vec{n}) dS \right\rangle + \int_{S_0} (\langle \boldsymbol{\sigma_2} \rangle \cdot \vec{n}) dS \tag{12}$$

Note that for the second order contribution the surface S_0 is time-invariant as a steady flow is assumed in the second simulation step. This contribution contains the acoustic radiation force which is caused by the nonzero time-averaged pressure $\langle p_2 \rangle$ and the Stokes' drag force caused by the nonzero time-averaged velocity $\langle \vec{u_2} \rangle$. Additionally, though the time-averaged first-order stress tensor itself is 0, integrating it over the time-varying surface of the swimmer $S(t)$ gives rise to a nonlinear term which can be obtained via the Leibniz-Reynolds transport theorem [5]. Physically this force originates from the harmonic motion of the swimmer in the varying first-order pressure and velocity fields. This force will be referred to as the LRTT force and is calculated using:

$$\left\langle \int_{S(t)} (\boldsymbol{\sigma_1} \cdot \vec{n}) dS \right\rangle = - \left\langle \int_{S(t)} \rho_0 \vec{u_1} \vec{u_1} \cdot \vec{n} dS \right\rangle \tag{13}$$

2.3.b Model description

The acoustofluidic simulations consist of two steps: one to solve for the time-harmonic first-order acoustic fields as described in equations (6) and (7) and another to solve for the second-order time-averaged acoustic streaming according to equations (8) and (9).

The first-order acoustic field around the swimmer was computed using the thermoviscous acoustics and solid mechanics modules for the fluid and swimmer, respectively. The physics of both modules were coupled using an acoustic-structure interaction boundary condition on the perimeter of the swimmer.

For this simulation the fluid medium was modeled as a rectangular domain of 1050μm by 600μm. A smaller domain size was chosen to limit the increase in computational load when solving for the more complex physics compared to the acoustics analysis. On the lower border of the domain a harmonically varying velocity was prescribed to model an acoustic perturbation in the form of a traveling wave. The amplitude of this velocity perturbation was normalized with respect to frequency to yield a similar magnitude of the resulting acoustic pressure field. This was done using a normalization function derived by fitting a curve to unscaled values of the acoustic pressure magnitude as a function of frequency. All other domain borders were modeled using perfectly matched layers to mimic an infinite domain.

The steady second-order acoustic streaming field was modeled on the same domain using a stationary study in the laminar flow module in COMSOL. In this case all boundaries of the fluid domain including that between the swimmer and the medium have been modeled using wall boundary conditions. The nonlinear source terms from the first order equations have been implemented using weak contributions applied to the fluid domain.

After solving for the first and second order fields successively the propulsive forces on the swimmer were determined. The force component due to the integration of the first-order stress tensor was calculated using the expression in equation (13). For the second-order force contributions the total fluid stress tensor in the steady acoustic streaming field was integrated over the swimmer surface. Additionally the viscous stress was integrated to discern the magnitude and direction of Stokes' drag force. The acoustic radiation force was computed as the difference of the total propulsive force and Stokes' drag force.

3 RESULTS

3.1 Structural analysis

The eigenmodes and the corresponding eigenfrequencies for the regular 180μm swimmer and the stingray I swimmer are shown in figure 2. For these swimmer designs the modes consist of harmonics of the tail.

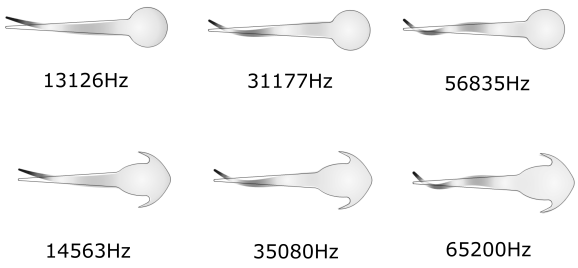

Fig. 2: Eigenmodes and corresponding frequencies of 180μm swimmer without protrusions (top) and stingray I swimmer (bottom)

For the protrusion-less swimmers elastic strain energy is plotted against the excitation frequency in figure 3. Changing swimmer tail size did not alter the shape of the eigenmodes, instead solely changing the frequencies at which these occur. Greater tail size results in a shift of the eigenmodes towards lower frequencies.

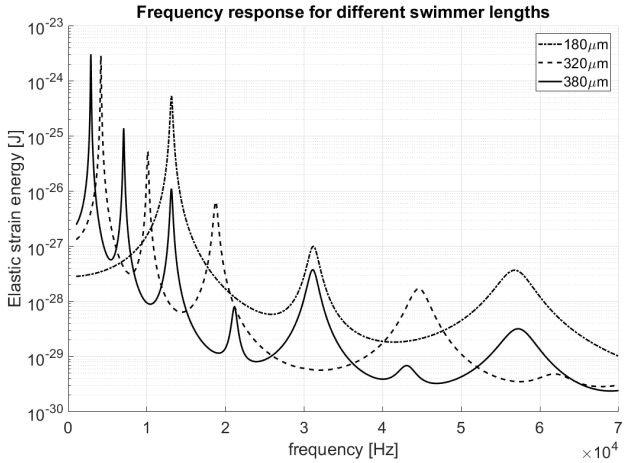

Fig. 3: Elastic strain energy of various size micro-swimmers without protrusions.

Contrary to the stingray I model, the large protrusions of the stingray II model introduce new vibrational modes as shown in figure 4. These modes show up as additional peaks in the frequency response plot of figure 5. Additionally the elastic strain energy of the protrusion-less 180μm swimmer was plotted for comparison reasons. It can be seen that the stingray I swimmer has an equal number of eigenfrequencies which are shifted to slightly higher frequencies compared to those of the protrusion-less swimmer.

Fig. 4: Eigenmodes and corresponding frequencies of stingray II swimmer

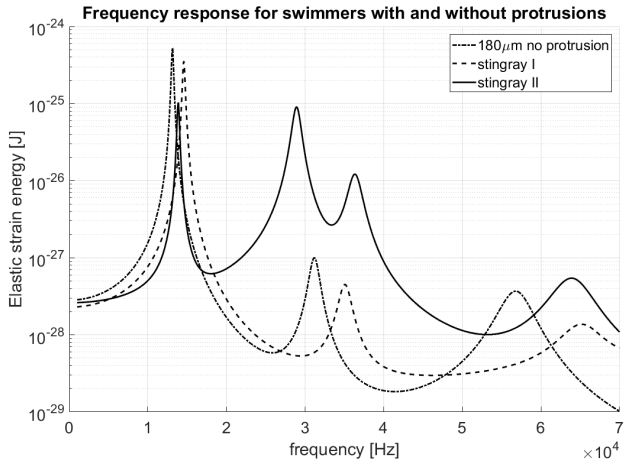

Fig. 5: Elastic strain energy of 180μm micro-swimmers with different protrusion sizes.

3.2 Acoustics

The eigenfrequencies in the acoustic model were lowered by a factor of 2 to 3 depending on swimmer design compared to the results obtained in the structural analysis. It was found that exciting the swimmer with an incident pressure field corresponding to these shifted eigenfrequencies indeed succeeded in producing the desired asymmetric motion. Pressure nodes are observed at the antinodes of the swimmer displacement wave as shown for the 180μm swimmer and stingray II swimmer in figure 6.

3.3 Acoustofluidics

In the results from the acoustofluidic analysis a great similarity was observed in the flow fields of the protrusion-less swimmers and the stingray I swimmer. For this reason only those results pertaining to the regular 180μm swimmer and the stingray II swimmer will be discussed.

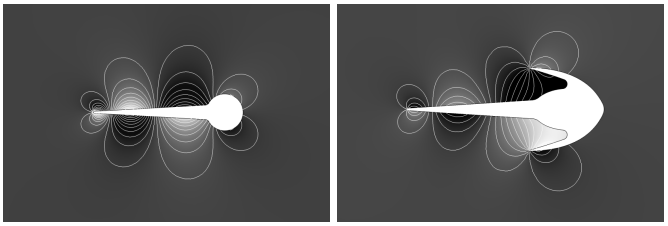

(a) 15202Hz (b) 36236hz

Fig. 6: Pressure fields around acoustically-actuated swimmers excited at eigenfrequencies

Evaluation of the forces on the swimmers at different excitation frequencies shows that the second-order contributions of the acoustic radiation force and Stokes' drag force are dominant over the first-order contributions from the integral in equation (13) by at least three orders of magnitude for the investigated frequencies. For this reason these first-order contributions will be neglected in the following discussion. As the force in the x direction longitudinal to the swimmer is much larger than that in the lateral y direction this will be the topic of discussion in the following.

For all swimmer designs the propulsive forces when using the aforementioned normalization to the first-order pressure field decrease with actuation frequency. The acoustic impedance of the swimmer material is of great influence on both the swimmer deformations and the propulsive forces. This can be illustrated by changing the mass density (and hence the acoustic impedance) of the swimmer and plotting the propulsive forces as in figure 7. Regular PDMS has a density of 970kg/m^3 and its acoustic impedance is very similar to that of water. This reduces scattering of incoming acoustic waves and leads the swimmer to behave similarly to the fluid around it [10]. Hence its movement consists predominantly of rigid-body motion with only small modal deformations.

By changing the density the relative magnitude of modal deformations becomes much greater as shown in the inset of figure 7. This change in deformation has an influence on both the direction and magnitude of the propulsive forces. As the influence of these modal vibrations on propulsive forces is the main focus of this research a mass density of 9700kg/m^3 was used for all of the following results.

To further investigate the effect of modal vibrations on

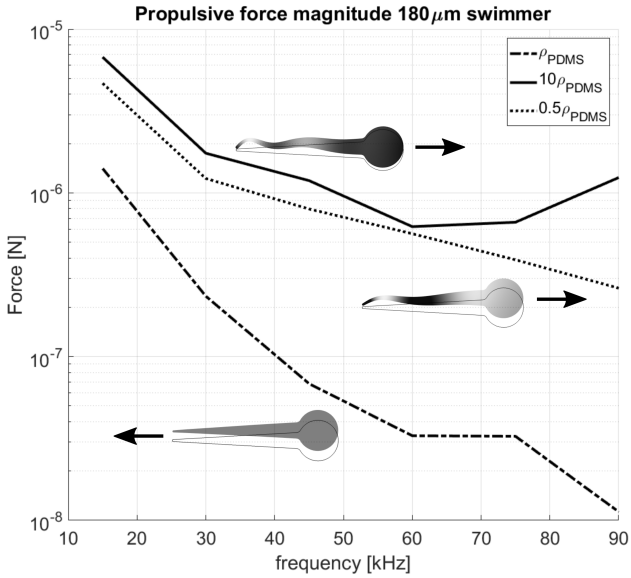

Fig. 7: Propulsive force magnitude in the x direction at various frequencies for the 180μm swimmer with different density values. The swimmer deformation at 30kHz is shown as an inset. The arrows next to the inset figures indicate the direction of the propulsive force.

the propulsive forces first a frequency sweep was carried out for the increased-density PDMS swimmers. Then propulsive forces were evaluated on a narrow range around the eigenfrequencies. The frequency response of the increased-density swimmers is shown in figure 8.

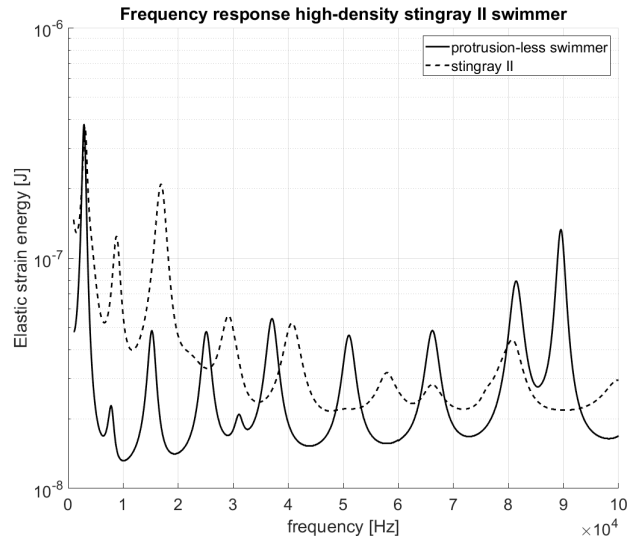

Fig. 8: Frequency response of the increased-density 180μm swimmer and stingray II swimmer

At low frequencies the effect of excitation at the eigenfrequencies (peaks of figure 8) is obscured by general tendency of a rapid decrease in propulsive

force with frequency until around 60kHz as seen in figure 7. Around higher eigenfrequencies an appreciable relation between large deformations and propulsive forces can be observed.

The second-order velocity field near the eigenfrequency of 81350Hz is shown in figure 9. Note the pair of vortices near the tail, which are also observed for the flow fields at the other eigenfrequencies of 66200Hz and 89950Hz.

Evaluating the propulsive forces near the eigenfrequencies of 66200Hz, 81350Hz and 89550Hz reveals a positive relationship between propulsive forces and elastic strain energy (deformation). The force components and elastic strain energy when exciting at these frequencies is shown on the top of row figure 11. It was found that an increased viscous (Stokes' drag) force contribution at the tail is primarily responsible for the increased propulsive forces at 66200Hz and 81350Hz as seen in figures 10a and 10b. At 89550Hz a sharp increase in acoustic radiation force acting on the front of the swimmer head causes an increase in total propulsive forces despite some rearward viscous force contributions as seen in figure 10c.

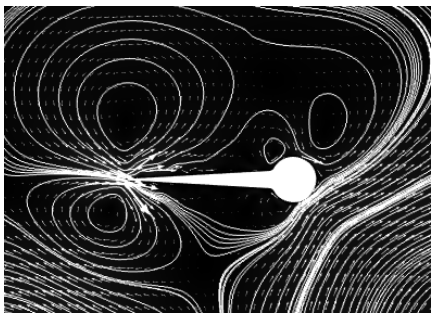

Fig. 9: Second-order velocity field at 81350Hz

The propulsive forces on the stingray II swimmer are plotted against frequency near the eigenfrequencies in the bottom of figure 11. At eigenfrequencies of 40700Hz and 66200Hz propulsive forces increase akin to the case of the regular 180μm swimmer, though the effect is less pronounced. However near the eigenfrequency at 80700Hz a decrease in propulsive forces occurs. The corresponding second-order velocity and pressure fields are shown in figure 12.

(a) 84000Hz

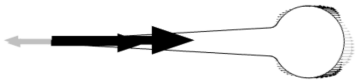

(b) Eigenfrequency of 81350Hz

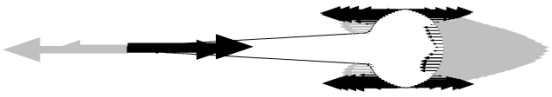

(c) Eigenfrequency of 89550Hz

Fig. 10: X-components of the acoustic radiation force (gray) and Stokes' drag force (black) on the protrusion-less swimmer surface

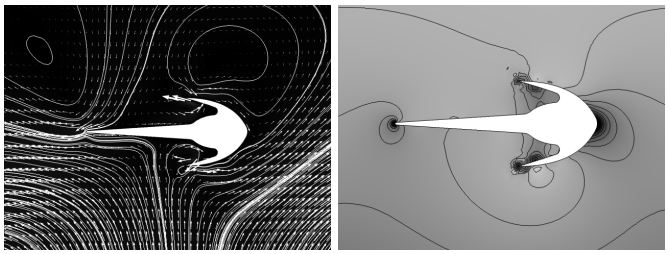

(a) Velocity (b) Pressure

Fig. 12: Second-order fields for the stingray II swimmer excited at its eigenfrequency of 80700Hz

The x-components of the acoustic radiation force and Stokes' drag force plotted on the swimmer surface as shown in figure 13.

For excitation frequencies above and below the eigenfrequency the acoustic radiation force has a positive component in the regions just behind the protrusions which disappears as the swimmer vibrates at resonance. Additionally a negative Stokes' drag force component appears at the protrusions.

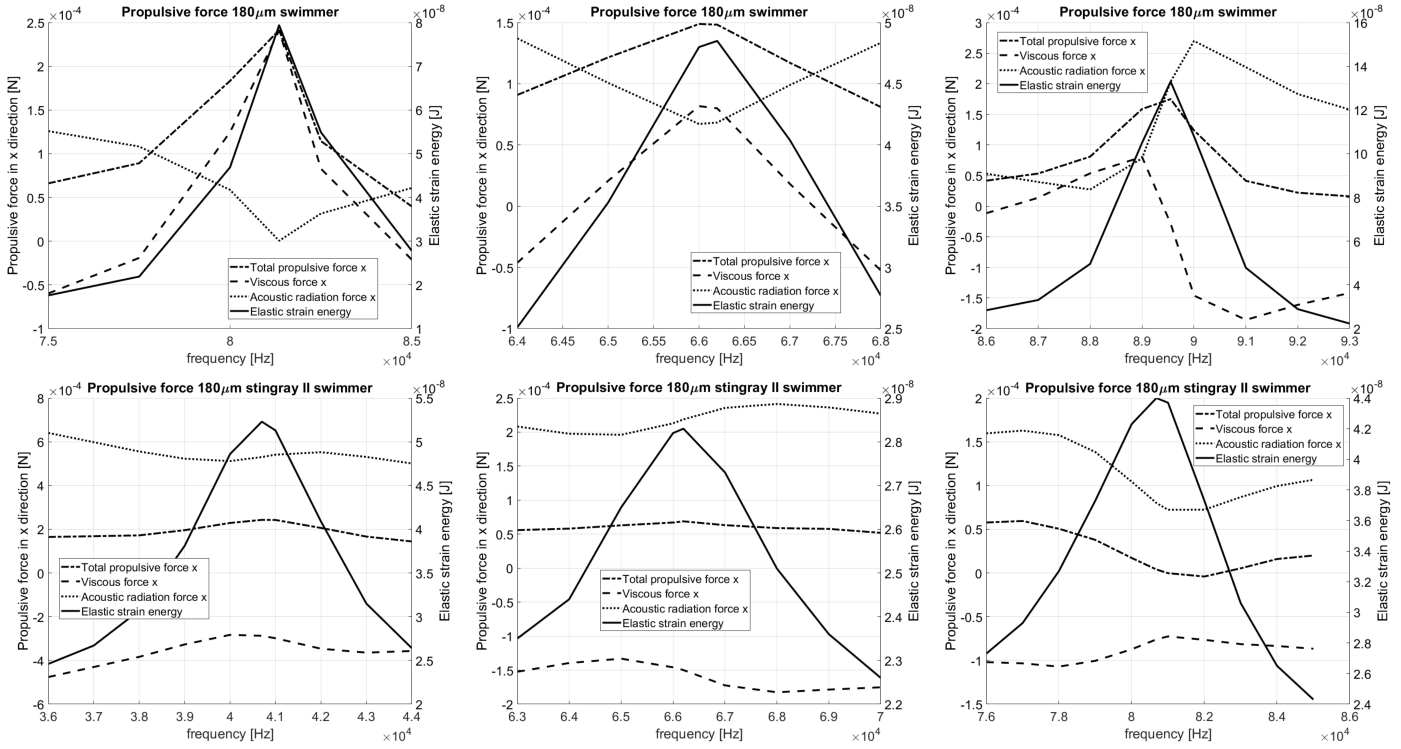

Fig. 11: Propulsive forces on the protrusion-less 180μm and stingray II swimmer.

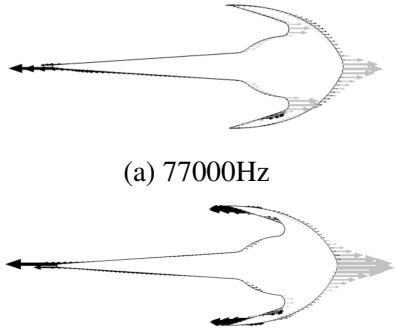

(a) 77000Hz

(b) Eigenfrequency of 80700Hz

Fig. 13: X-components of the acoustic radiation force (gray) and Stokes' drag force (black) on the stingray II swimmer surface

4 DISCUSSION

A structural analysis of swimmer designs shows that lengthening the swimmer tail or adding small protrusions shifts eigenfrequencies to lower values. This can be explained by the decreased specific stiffness of the long-tailed designs. Similarly the lower eigenfrequencies of the stingray I design can be explained by the increased mass from the larger head size while the stiffness of the tail remains about the same as in the regular 180μm model. Large protrusions as in the stingray II design lead to additional vibrational modes in which the protrusions vibrate.

A similar rationale can be used to explain the lowering of eigenfrequencies for all designs with the addition of fluid in the acoustic analysis. This surrounding medium must move with the swimmer as it vibrates, effectively adding mass to the system and hence lowering the eigenfrequencies.

From the acoustofluidic analysis the acoustic impedance of the swimmer material was found to be relevant for the first and second order streaming fields as it influences the scattering of acoustic waves as they hit the swimmer. It is expected that manipulating the acoustic impedance of different parts of the swimmer may provide further control over the acoustic fields and propulsive forces. This is a promising topic for new research to further gain insight into possible means of controlling synthetic micro-swimmers using acoustics.

Excitation at the eigenfrequencies in general results in an increase of propulsive forces for the 180μm swimmer which most readily presents itself in the viscous force term. An exception is the eigenfrequency of 89550Hz where the acoustic radiation force is responsible for the increased propulsive force, in fact counteracting a rearward viscous force contribution.

A physical explanation for this increase in viscous forces pointing towards the head may be found in the position of the two counter-rotating vortices at the tail tip. These vortices produce a high-velocity flow along the tail tip in the direction of the head as seen in figure 9. At frequencies above or below the eigenfrequency the alignment of these vortices is skewed, yielding a smaller flow around the tail-tip. This explains the increase in the viscous force term at the eigenfrequency which is visible in figure 10. In the unique case of excitation at 89550Hz the described pairs of vortices occur at both sides of the head as well as the tail, which explains the ‚rearward viscous force at the back of the head. The vortices to the front of the head create a low pressure region by increasing flow velocity, hence the increased acoustic radiation force in this area as seen in figure 10c.

In contrast, the stingray II design exhibits a decrease in total propulsive force at its eigenfrequency of 80700Hz. Both the acoustic radiation force and Stokes' drag force contribute to this phenomenon. At excitation frequencies above and below the eigenfrequency high-pressure regions behind the protrusions yield a headward-facing acoustic radiation force. Excitation at the eigenfrequency results in a vibration which leads to stagnant flow regions immediately behind the protrusions, explaining the reduced headward pressure force. The increase in tailward viscous forces at the protrusion tips may be explained by the strong vortex formation in these areas when the tips are made to vibrate at resonance.

It is noted that though the 2D analyses performed are sufficient to illustrate the effect of resonance vibrations on propulsive forces, this simplification influences both the mode shapes and resonance frequencies of the swimmer as well as the acoustic fields. Future research is required to evaluate 3D effects.

5 CONCLUSION

Structural mechanics and pressure acoustics simulations show that external actuation can induce micro-swimmer resonance vibrations mimicking the movements of biological swimmers. The frequencies at which these vibrations occur vary with swimmer dimensions and geometry. Placing the swimmer in a medium has the effect of lowering the frequencies at which the resonance modes occur due to the additional inertia of the surrounding fluid. Knowledge of these effects could be used to accommodate swimmer eigenfrequencies to those of a transducer.

Applying a perturbation approach to the linearized continuity and Navier-Stokes equations simplifies the acoustofluidic numerical problem by decoupling the first-order time-harmonic acoustic fields and the second-order streaming fields. Thermoviscous acoustics simulations revealed that the swimmer's acoustic impedance, geometry and vibrational modes have a strong influence on the streaming fields and directionality of the propulsive forces. Exciting swimmers at their resonance frequencies in general increases positive propulsive forces due to the alignment of vortices at the tail. Addition of protrusions to the swimmer head complicates the relationship between resonances and propulsive forces, producing some modes in which a negative force contribution is induced as the streaming field pressure drops behind the oscillating protrusions. This modal dependence of directionality suggests the possibility of controlling swimmers by matching excitation frequency to particular swimmer modes.

REFERENCES

1. K. J. Rao, F. Li, L. Meng, H. Zheng, F. Cai, and W. Wang, A force to be reckoned with: A review of synthetic microswimmers powered by ultrasound, *Small*, (2015), 11(24):2836–2846.
2. B. Lautrup, *Physics of Continuous Matter*, The Niels Bohr Institute, Copenhagen, Denmark, (2004).
3. E.M. Purcell, Life at low reynolds number, *American Journal of Physics*, (1977), 45:3–11.
4. G. Destgeer and H.J. Sung, Recent advances in microfluidic actuation and micro-object manipulation via surface acoustic waves, *Lab Chip*, (2015), 15:2722–2738.
5. A. Lamprecht, *Optical Traps for Characterising Acoustically Induced Forces and Torques Acting on Microparticles*, PhD thesis, ETH Zurich, (2017).
6. D. Ahmed, T. Baasch, B. Jang, S. Pane, J. Dual, and Bradley J. Nelson, Artificial swimmers propelled by acoustically activated flagella, *Nano Letters*, (2016), 16:4968–4974.
7. H. Bruus, Acoustofluidics 2: Perturbation theory and ultrasound resonance modes, *Lab on a chip*, 1 2012, 12:20–28.
8. M. Wiklund, R. Green, and M. Ohlin, Acoustofluidics 14: Applications of acoustic streaming in microfluidic devices, *Lab on a chip*, (2012), 12:2438–2451.
9. W. Mason, *Physical Acoustics: Properties of Gases, Liquids and Solutions*, Academic Press, Cambridge, MA, (1965).
10. M. Schwartz, *The Physics of Waves*, Harvard University, Cambridge, MA, (2015).

A MATERIAL PROPERTIES

Table 1: Thermoviscous acoustics fluid properties

Property	Symbol	Value
Equilibrium mass density	ρ_0	1000[kg/m^3]
Equilibrium pressure	p_0	1 [atm]
Equilibrium temperature	T_0	293.15[K]
Dynamic viscosity	μ	8.5e-4[Pa·s]
Bulk viscosity	μ_B	2.4e-3[Pa·s]
Thermal conductivity	k	0.61[W/(m·K)]
Heat capacity at constant pressure	C_p	4.18e3[J/(kg·K)]
Coefficient of thermal expansion	α_p	2.75e-4[1/K]
Isentropic compressibility	β_s	4.45e-10[1/Pa]
Ratio of specific heats	γ	1.012

Table 2: Solid mechanics properties

Property	Symbol	Value
Young's modulus	E	750[kPa]
Poisson's ratio	ν	0.49
Mass density	ρ_{pdms}	970[kg/m^3]

Table 3: Laminar flow fluid properties

Property	Symbol	Value
Mass density	ρ	1000[kg/m^3]
Dynamic viscosity	μ	8.5e-4[Pa·s]

B ORDER OF MAGNITUDE OF PROPULSIVE FORCES

Force component	Order of magnitude
Acoustic radiation force	-2 to -7
Stokes' drag force	-2 to -7
LRTT force	-10 to -12